

A Study of $W^+W^-\gamma$ Events at LEP

The OPAL Collaboration

Abstract

A study of W^+W^- events accompanied by hard photon radiation, $E_\gamma > 2.5$ GeV, produced in e^+e^- collisions at LEP is presented. Events consistent with being two on-shell W-bosons and an isolated photon are selected from 681 pb^{-1} of data recorded at $180 \text{ GeV} < \sqrt{s} < 209 \text{ GeV}$. From the sample of 187 selected $W^+W^-\gamma$ candidates with photon energies greater than 2.5 GeV, the $W^+W^-\gamma$ cross-section is determined at five values of \sqrt{s} . The results are consistent with the Standard Model expectation. Averaging over all energies, the ratio of the observed cross-section to the Standard Model expectation is

$$R(\text{data/SM}) = 0.99 \pm 0.09 \pm 0.04,$$

where the errors represent the statistical and systematic uncertainties respectively. These data provide constraints on the related $\mathcal{O}(\alpha)$ systematic uncertainties on the measurement of the W-boson mass at LEP. Finally, the data are used to derive 95 % confidence level upper limits on possible anomalous contributions to the $W^+W^-\gamma\gamma$ and $W^+W^-Z^0\gamma$ vertices:

$$\begin{aligned} -0.020 \text{ GeV}^{-2} < a_0/\Lambda^2 < 0.020 \text{ GeV}^{-2}, \\ -0.053 \text{ GeV}^{-2} < a_c/\Lambda^2 < 0.037 \text{ GeV}^{-2}, \\ -0.16 \text{ GeV}^{-2} < a_n/\Lambda^2 < 0.15 \text{ GeV}^{-2}, \end{aligned}$$

where Λ represents the energy scale for new physics and a_0 , a_c and a_n are dimensionless coupling constants.

(To be Submitted to Physics Letters B)

The OPAL Collaboration

G. Abbiendi², C. Ainsley⁵, P.F. Åkesson³, G. Alexander²², J. Allison¹⁶, P. Amaral⁹,
G. Anagnostou¹, K.J. Anderson⁹, S. Arcelli², S. Asai²³, D. Axen²⁷, G. Azuelos^{18,a}, I. Bailey²⁶,
E. Barberio^{8,p}, R.J. Barlow¹⁶, R.J. Batley⁵, P. Bechtel²⁵, T. Behnke²⁵, K.W. Bell²⁰, P.J. Bell¹,
G. Bella²², A. Bellerive⁶, G. Benelli⁴, S. Bethke³², O. Biebel³¹, O. Boeriu¹⁰, P. Bock¹¹,
M. Boutemour³¹, S. Braibant⁸, L. Brigliadori², R.M. Brown²⁰, K. Buesser²⁵, H.J. Burckhart⁸,
S. Campana⁴, R.K. Carnegie⁶, B. Caron²⁸, A.A. Carter¹³, J.R. Carter⁵, C.Y. Chang¹⁷,
D.G. Charlton¹, A. Csilling²⁹, M. Cuffiani², S. Dado²¹, A. De Roeck⁸, E.A. De Wolf^{8,s},
K. Desch²⁵, B. Dienes³⁰, M. Donkers⁶, J. Dubbert³¹, E. Duchovni²⁴, G. Duckeck³¹,
I.P. Duerdoth¹⁶, E. Etzion²², F. Fabbri², L. Feld¹⁰, P. Ferrari⁸, F. Fiedler³¹, I. Fleck¹⁰, M. Ford⁵,
A. Frey⁸, A. Fürtjes⁸, P. Gagnon¹², J.W. Gary⁴, G. Gaycken²⁵, C. Geich-Gimbel³,
G. Giacomelli², P. Giacomelli², M. Giunta⁴, J. Goldberg²¹, E. Gross²⁴, J. Grunhaus²²,
M. Gruwé⁸, P.O. Günther³, A. Gupta⁹, C. Hajdu²⁹, M. Hamann²⁵, G.G. Hanson⁴, K. Harder²⁵,
A. Harel²¹, M. Harin-Dirac⁴, M. Hauschild⁸, C.M. Hawkes¹, R. Hawkings⁸, R.J. Hemingway⁶,
C. Hensel²⁵, G. Herten¹⁰, R.D. Heuer²⁵, J.C. Hill⁵, K. Hoffman⁹, D. Horváth^{29,c},
P. Igo-Kemenes¹¹, K. Ishii²³, H. Jeremie¹⁸, P. Jovanovic¹, T.R. Junk⁶, N. Kanaya²⁶,
J. Kanzaki^{23,u}, G. Karapetian¹⁸, D. Karlen²⁶, K. Kawagoe²³, T. Kawamoto²³, R.K. Keeler²⁶,
R.G. Kellogg¹⁷, B.W. Kennedy²⁰, D.H. Kim¹⁹, K. Klein^{11,t}, A. Klier²⁴, S. Kluth³²,
T. Kobayashi²³, M. Kobel³, S. Komamiya²³, L. Kormos²⁶, T. Krämer²⁵, P. Krieger^{6,l}, J. von
Krogh¹¹, K. Kruger⁸, T. Kuhl²⁵, M. Kupper²⁴, G.D. Lafferty¹⁶, H. Landsman²¹, D. Lanske¹⁴,
J.G. Layter⁴, A. Leins³¹, D. Lellouch²⁴, J. Letts^o, L. Levinson²⁴, J. Lillich¹⁰, S.L. Lloyd¹³,
F.K. Loebinger¹⁶, J. Lu^{27,w}, J. Ludwig¹⁰, A. Macpherson^{28,i}, W. Mader³, S. Marcellini²,
A.J. Martin¹³, G. Masetti², T. Mashimo²³, P. Mättig^m, W.J. McDonald²⁸, J. McKenna²⁷,
T.J. McMahan¹, R.A. McPherson²⁶, F. Meijers⁸, W. Menges²⁵, F.S. Merritt⁹, H. Mes^{6,a},
A. Michelini², S. Mihara²³, G. Mikenberg²⁴, D.J. Miller¹⁵, S. Moed²¹, W. Mohr¹⁰, T. Mori²³,
A. Mutter¹⁰, K. Nagai¹³, I. Nakamura^{23,v}, H. Nanjo²³, H.A. Neal³³, R. Nisius³², S.W. O’Neale¹,
A. Oh⁸, A. Okpara¹¹, M.J. Oreglia⁹, S. Orito^{23,*}, C. Pahl³², G. Pásztor^{4,g}, J.R. Pater¹⁶,
G.N. Patrick²⁰, J.E. Pilcher⁹, J. Pinfold²⁸, D.E. Plane⁸, B. Poli², J. Polok⁸, O. Pooth¹⁴,
M. Przybycien^{8,n}, A. Quadt³, K. Rabbertz^{8,r}, C. Rembser⁸, P. Renkel²⁴, J.M. Roney²⁶,
S. Rosati³, Y. Rozen²¹, K. Runge¹⁰, K. Sachs⁶, T. Saeki²³, E.K.G. Sarkisyan^{8,j}, A.D. Schaile³¹,
O. Schaile³¹, P. Scharff-Hansen⁸, J. Schieck³², T. Schörner-Sadenius⁸, M. Schröder⁸,
M. Schumacher³, C. Schwick⁸, W.G. Scott²⁰, R. Seuster^{14,f}, T.G. Shears^{8,h}, B.C. Shen⁴,
P. Sherwood¹⁵, G. Siroli², A. Skuja¹⁷, A.M. Smith⁸, R. Sobie²⁶, S. Söldner-Rembold^{16,d},
F. Spano⁹, A. Stahl³, K. Stephens¹⁶, D. Strom¹⁹, R. Ströhmer³¹, S. Tarem²¹, M. Tasevsky⁸,
R.J. Taylor¹⁵, R. Teuscher⁹, M.A. Thomson⁵, E. Torrence¹⁹, D. Toya²³, P. Tran⁴, I. Trigger⁸,
Z. Trócsányi^{30,e}, E. Tsur²², M.F. Turner-Watson¹, I. Ueda²³, B. Ujvári^{30,e}, C.F. Vollmer³¹,
P. Vannerem¹⁰, R. Vértesi³⁰, M. Verzocchi¹⁷, H. Voss^{8,q}, J. Vossebeld^{8,h}, D. Waller⁶, C.P. Ward⁵,
D.R. Ward⁵, P.M. Watkins¹, A.T. Watson¹, N.K. Watson¹, P.S. Wells⁸, T. Wengler⁸,
N. Wermes³, D. Wetterling¹¹, G.W. Wilson^{16,k}, J.A. Wilson¹, G. Wolf²⁴, T.R. Wyatt¹⁶,
S. Yamashita²³, D. Zer-Zion⁴, L. Zivkovic²⁴

¹School of Physics and Astronomy, University of Birmingham, Birmingham B15 2TT, UK

²Dipartimento di Fisica dell’ Università di Bologna and INFN, I-40126 Bologna, Italy

³Physikalisches Institut, Universität Bonn, D-53115 Bonn, Germany

- ⁴Department of Physics, University of California, Riverside CA 92521, USA
- ⁵Cavendish Laboratory, Cambridge CB3 0HE, UK
- ⁶Ottawa-Carleton Institute for Physics, Department of Physics, Carleton University, Ottawa, Ontario K1S 5B6, Canada
- ⁸CERN, European Organisation for Nuclear Research, CH-1211 Geneva 23, Switzerland
- ⁹Enrico Fermi Institute and Department of Physics, University of Chicago, Chicago IL 60637, USA
- ¹⁰Fakultät für Physik, Albert-Ludwigs-Universität Freiburg, D-79104 Freiburg, Germany
- ¹¹Physikalisches Institut, Universität Heidelberg, D-69120 Heidelberg, Germany
- ¹²Indiana University, Department of Physics, Bloomington IN 47405, USA
- ¹³Queen Mary and Westfield College, University of London, London E1 4NS, UK
- ¹⁴Technische Hochschule Aachen, III Physikalisches Institut, Sommerfeldstrasse 26-28, D-52056 Aachen, Germany
- ¹⁵University College London, London WC1E 6BT, UK
- ¹⁶Department of Physics, Schuster Laboratory, The University, Manchester M13 9PL, UK
- ¹⁷Department of Physics, University of Maryland, College Park, MD 20742, USA
- ¹⁸Laboratoire de Physique Nucléaire, Université de Montréal, Montréal, Québec H3C 3J7, Canada
- ¹⁹University of Oregon, Department of Physics, Eugene OR 97403, USA
- ²⁰CLRC Rutherford Appleton Laboratory, Chilton, Didcot, Oxfordshire OX11 0QX, UK
- ²¹Department of Physics, Technion-Israel Institute of Technology, Haifa 32000, Israel
- ²²Department of Physics and Astronomy, Tel Aviv University, Tel Aviv 69978, Israel
- ²³International Centre for Elementary Particle Physics and Department of Physics, University of Tokyo, Tokyo 113-0033, and Kobe University, Kobe 657-8501, Japan
- ²⁴Particle Physics Department, Weizmann Institute of Science, Rehovot 76100, Israel
- ²⁵Universität Hamburg/DESY, Institut für Experimentalphysik, Notkestrasse 85, D-22607 Hamburg, Germany
- ²⁶University of Victoria, Department of Physics, P O Box 3055, Victoria BC V8W 3P6, Canada
- ²⁷University of British Columbia, Department of Physics, Vancouver BC V6T 1Z1, Canada
- ²⁸University of Alberta, Department of Physics, Edmonton AB T6G 2J1, Canada
- ²⁹Research Institute for Particle and Nuclear Physics, H-1525 Budapest, P O Box 49, Hungary
- ³⁰Institute of Nuclear Research, H-4001 Debrecen, P O Box 51, Hungary
- ³¹Ludwig-Maximilians-Universität München, Sektion Physik, Am Coulombwall 1, D-85748 Garching, Germany
- ³²Max-Planck-Institute für Physik, Föhringer Ring 6, D-80805 München, Germany
- ³³Yale University, Department of Physics, New Haven, CT 06520, USA

^a and at TRIUMF, Vancouver, Canada V6T 2A3

^c and Institute of Nuclear Research, Debrecen, Hungary

^d and Heisenberg Fellow

^e and Department of Experimental Physics, Lajos Kossuth University, Debrecen, Hungary

^f and MPI München

^g and Research Institute for Particle and Nuclear Physics, Budapest, Hungary

^h now at University of Liverpool, Dept of Physics, Liverpool L69 3BX, U.K.

ⁱ and CERN, EP Div, 1211 Geneva 23

^j and Manchester University

^k now at University of Kansas, Dept of Physics and Astronomy, Lawrence, KS 66045, U.S.A.

^l now at University of Toronto, Dept of Physics, Toronto, Canada

^m current address Bergische Universität, Wuppertal, Germany

ⁿ now at University of Mining and Metallurgy, Cracow, Poland

^o now at University of California, San Diego, U.S.A.

^p now at Physics Dept Southern Methodist University, Dallas, TX 75275, U.S.A.

^q now at IPHE Université de Lausanne, CH-1015 Lausanne, Switzerland

^r now at IEKP Universität Karlsruhe, Germany

^s now at Universitaire Instelling Antwerpen, Physics Department, B-2610 Antwerpen, Belgium

^t now at RWTH Aachen, Germany

^u and High Energy Accelerator Research Organisation (KEK), Tsukuba, Ibaraki, Japan

^v now at University of Pennsylvania, Philadelphia, Pennsylvania, USA

^w now at TRIUMF, Vancouver, Canada

* Deceased

1 Introduction

The W^+W^- pair production cross-section has been precisely measured at LEP over a range of centre-of-mass energies [1–3]. The data are well described by the Standard Model (SM) expectation [4, 5]. The good agreement between experiment and theory is only obtained once factorizable and non-factorizable $\mathcal{O}(\alpha)$ photonic corrections are included in the theoretical calculations (see for example [6] and references therein). The inclusion of real and virtual photonic corrections in the YFSWW [4] and RacoonWW [5] programs has reduced the theoretical uncertainty on the CC03 $e^+e^- \rightarrow W^+W^-$ cross-section¹ to below 0.5 % [6]. Uncertainties in these $\mathcal{O}(\alpha)$ corrections may lead to small, but non-negligible, systematic uncertainties in the determination of the W-boson mass, M_W , at LEP [7]. This paper presents a study of the process $e^+e^- \rightarrow W^+W^-\gamma$ and thus probes the modelling of real photonic corrections to the W^+W^- pair creation process. The data are used to obtain measurements of the $e^+e^- \rightarrow W^+W^-\gamma$ cross-section within a restricted phase-space region, $\hat{\sigma}_{WW\gamma}$, for $180 \text{ GeV} < \sqrt{s} < 209 \text{ GeV}$.

In the SM, photon radiation in the W^+W^- production process at LEP can be categorized into four main classes of diagrams: initial state radiation (ISR); final state radiation (FSR) from a lepton; FSR from the quark or from the associated parton shower; and bremsstrahlung from one of the intermediate W-bosons, referred to as WSR. At LEP energies WSR has a significant effect only through interference with ISR. Experimentally photons arising from decays of hadrons in a jet are indistinguishable from FSR photons from a quark or parton shower. For this reason, and due to the relatively large uncertainties in the Monte Carlo modelling of photon production in the parton shower, all photons associated with hadronic jets (from hadron decay and FSR) are considered background for the measurements of $\hat{\sigma}_{WW\gamma}$.

The measurements of the $W^+W^-\gamma$ cross-section are compared with the predictions of the KORALW [8], KandY [9] (the concurrent Monte Carlo KORALW1.51 and YFSWW3) and RacoonWW [5] programs. These comparisons are used to obtain the first data-driven estimate of the systematic uncertainty on M_W due to the Monte Carlo description of real photon radiation in W^+W^- events.

In addition, the $W^+W^-\gamma$ final state is sensitive to possible anomalous $W^+W^-\gamma\gamma$ and $W^+W^-Z^0\gamma$ quartic gauge boson couplings (QGCs). At LEP energies the contribution of the

¹CC03 refers to the three doubly resonant diagrams for $e^+e^- \rightarrow W^+W^-$.

SM QGC diagram is negligible. The data presented in this paper are used to place upper limits on the size of possible anomalous QGCs. These limits are more than a factor three tighter than previous OPAL results from $e^+e^- \rightarrow W^+W^-\gamma$ [10] and are consistent with other measurements [11].

2 The OPAL Detector, Data Samples and Monte Carlo

2.1 The OPAL Detector

The OPAL detector includes a 3.7 m diameter tracking volume within a 0.435 T axial magnetic field. The tracking detectors include a silicon micro-vertex detector, a high precision gas vertex detector and a large volume gas jet chamber. The tracking acceptance corresponds to approximately $|\cos\theta| < 0.95$ (for the track quality cuts used in this study)². Lying outside the solenoid, the electromagnetic calorimeter (ECAL) consisting of 11 704 lead glass blocks has full acceptance in the range $|\cos\theta| < 0.98$ and a relative energy resolution of approximately 6 % for 10 GeV photons. The magnet return yoke is instrumented with streamer tubes which serve as the hadronic calorimeter. Muon chambers outside the hadronic calorimeter provide muon identification in the range $|\cos\theta| < 0.98$. A detailed description of the OPAL detector can be found in [12].

2.2 Data Sample

During LEP 2 operation the centre-of-mass energy was increased from 161 GeV to 209 GeV in several steps. The total integrated luminosity of the data sample considered in this paper, evaluated using small angle Bhabha scattering events observed in the silicon tungsten forward calorimeter [13], is $(681 \pm 2) \text{ pb}^{-1}$. For the purpose of measuring the $W^+W^-\gamma$ cross-section these data are divided into the five \sqrt{s} ranges listed in Table 1. These ranges reflect the main energy steps as the centre-of-mass energy was increased during LEP2 operation. The data recorded at 161 GeV and 172 GeV, corresponding to a total integrated luminosity of 20 pb^{-1} , are not used here.

Range/GeV	$\langle \sqrt{s} \rangle$ /GeV	\mathcal{L} /pb ⁻¹
180.0–185.0	182.68	57.2
188.0–189.0	188.63	183.1
191.0–196.0	194.44	105.7
199.0–204.0	200.21	114.1
204.0–209.0	205.92	220.6

Table 1: The energy binning used for the $W^+W^-\gamma$ cross-section measurements. The \sqrt{s} range covered by each bin, the mean luminosity weighted value of \sqrt{s} and the corresponding integrated luminosity, \mathcal{L} , are listed.

²The OPAL right-handed coordinate system is defined such that the origin is at the centre of the detector and the z axis points along the direction of the e^- beam; θ is the polar angle with respect to the z axis.

2.3 Monte Carlo

A number of Monte Carlo (MC) samples, all including a full simulation [14] of the OPAL detector, are used to simulate the SM signal and background processes. For this paper the main MC samples for the process $e^+e^- \rightarrow W^+W^-\gamma$ were generated using the Kandy [9] program and, unless otherwise specified, the SM expectations for the $e^+e^- \rightarrow W^+W^-\gamma$ cross-section refer to the Kandy prediction. Kandy includes exact $\mathcal{O}(\alpha)$ YFS exponentiation [15] for the W^+W^- production process, with $\mathcal{O}(\alpha)$ electroweak non-leading (NL) corrections combined with YFS exponentiated $\mathcal{O}(\alpha^3)$ leading logarithm (LL) initial state radiation. Final state radiation from leptons is implemented in PHOTOS [16] and radiation from the quark induced parton-shower is performed by JETSET [17]. The most notable improvements over the KORALW program are the leading non-factorizable corrections in the Screened Coulomb ansatz [18], the inclusion of bremsstrahlung from the W-pairs (WSR), and the implementation of $\mathcal{O}(\alpha)$ electroweak NL corrections.

The KORALW program [8] is used to simulate the background from four-fermion final states which are incompatible with coming from the decays of two W-bosons (*e.g.* $e^+e^- \rightarrow q\bar{q}\mu^+\mu^-$). The two-fermion background processes, $e^+e^- \rightarrow Z^0/\gamma \rightarrow q\bar{q}$ and $e^+e^- \rightarrow Z^0/\gamma \rightarrow \tau^+\tau^-$, are simulated using KK2F [19]. The background in the $W^+W^-\gamma$ event selection from multi-peripheral two-photon diagrams was found to be negligible.

In addition, the RacoonWW program [5] is used in the Improved Born Approximation (IBA) mode to obtain independent predictions of the cross-sections for $e^+e^- \rightarrow W^+W^-\gamma$ and $e^+e^- \rightarrow 4f\gamma$. In this mode all lowest order diagrams contributing to $e^+e^- \rightarrow W^+W^-\gamma$ are included. The EEWG program [20] is used to obtain predicted cross-sections in the presence of anomalous QGCs which are then used to extract experimental limits on the anomalous contributions to the $W^+W^-\gamma\gamma$ and $W^+W^-Z^0\gamma$ vertices.

3 $W^+W^-\gamma$ Signal Definition

The process $e^+e^- \rightarrow W^+W^-\gamma$ results in a four-fermion plus photon final state, $f_1\bar{f}_2f_3\bar{f}_4\gamma$, where the fermion flavours are appropriate for W-decay. In the SM, photons are radiated in several classes of diagrams corresponding to ISR, FSR from both charged leptons and quarks, radiation from the W-boson (WSR) and the Standard Model QGC diagram. The invariant mass distributions of the fermions are different for the different radiation processes. In the case of ISR, the $f_1\bar{f}_2$ and $f_3\bar{f}_4$ systems are produced with invariant masses close to M_W . In the case of FSR, the $f_1\bar{f}_2\gamma$ and $f_3\bar{f}_4$ combinations or the $f_1\bar{f}_2$ and $f_3\bar{f}_4\gamma$ combinations give invariant masses close to the W-boson mass. For photon energies $E_\gamma > \Gamma_W$, where Γ_W is the W-boson width, events from FSR tend to occupy a different kinematic region from those arising from the ISR or QGC diagrams. Consequently, interference between FSR and ISR/QGC diagrams is suppressed. At LEP energies the effect of WSR is only significant through interference with ISR; the WSR diagrams are only of relevance to the region of phase-space populated by ISR diagrams.

Only part of the $W^+W^-\gamma$ phase-space is accessible experimentally and, therefore, it is necessary to define a specific region of phase-space in which the cross-section will be measured. The definition of the signal region is chosen to be well matched to the experimental sensitivity. In addition, by defining the cross-section to correspond to a region of four-fermion phase-space dominated by the doubly resonant W^+W^- production (CC03) diagrams, contributions from other interfering diagrams can be made small. In this way, the experimental results can be

compared with both the predictions of calculations implementing all four-fermion diagrams and with calculations implementing only CC03 diagrams. Finally, invariant mass cuts are imposed to reduce the contribution of FSR both from quarks and from leptons. This is desirable for two reasons. Firstly, any new physics is unlikely to manifest itself in a modification of FSR. Secondly, it reduces modelling uncertainties which are potentially large in the case of FSR from the quark-induced parton shower.

In this paper, the $W^+W^-\gamma \rightarrow f_1\bar{f}_2f_3\bar{f}_4\gamma$ cross-section, denoted by $\hat{\sigma}_{WW\gamma}$, is measured for:

- $E_\gamma > 2.5$ GeV, where E_γ is the photon energy.
- $|\cos\theta_\gamma| < 0.975$, where $\cos\theta_\gamma$ is the cosine of the polar angle of the photon.
- $\cos\theta_{\gamma f} < 0.90$, where $\cos\theta_{\gamma f}$ is the cosine of the minimum angle between the photon and any of the charged fermions in the four-fermion final state.
- $|\cos\theta_\ell| < 0.95$, where $|\cos\theta_\ell|$ is the modulus of the cosine of the polar angle of the charged lepton in the $W^+W^- \rightarrow q\bar{q}\ell\bar{\nu}_\ell$ final state. In the $W^+W^- \rightarrow \ell^+\nu_\ell\ell^-\bar{\nu}_\ell$ final state this requirement applies to both of the charged leptons.
- $|M_{f_1\bar{f}_2} - M_W|$ and $|M_{f_3\bar{f}_4} - M_W| < 3\Gamma_W$, where $M_{f_1\bar{f}_2}$ and $M_{f_3\bar{f}_4}$ are the invariant masses of fermions consistent with being from the decays of the W^- or W^+ .

The first three requirements are closely matched to the ability to reconstruct a pure sample of isolated photons in the OPAL detector. The requirement on the polar angle of the charged leptons from W -decay is imposed because the W^+W^- event selection becomes significantly less efficient beyond the acceptance of the tracking chambers. It also reduces contributions from interfering four-fermion background diagrams such as the t -channel process $e^+e^- \rightarrow We\bar{\nu}_e$. The cut on the invariant masses of the fermion pairs further reduces the (interfering) four-fermion backgrounds and suppresses the contribution of FSR to the signal region. Due to the finite jet width, jets are detected over the full polar angle acceptance and therefore there is no explicit requirement on the polar angle of the quark.

In the above definition of the signal, all requirements are made on generator level quantities. Generator level refers to the true four-momenta of particles in the $f_1\bar{f}_2f_3\bar{f}_4\gamma$ final state. The cross-section within the above kinematic cuts, $\hat{\sigma}_{WW\gamma}$, is dominated by doubly-resonant W^+W^- production. For example, the difference between the cross-section for the full set of $4f\gamma$ diagrams relative to cross-section for the CC03 diagrams alone is less than 0.5 % (calculated using the IBA implemented in RacoonWW [5]).

4 $W^+W^-\gamma$ Event Selection

The selection of $W^+W^-\gamma$ events proceeds in three stages: selection of W^+W^- events, photon identification, and background rejection using kinematic information. All W^+W^- final states are used in this study.

4.1 W^+W^- Selection

The $W^+W^- \rightarrow \ell^+\nu_\ell\ell^-\bar{\nu}_\ell$, $W^+W^- \rightarrow q\bar{q}\ell\bar{\nu}_\ell$ and $W^+W^- \rightarrow q\bar{q}q\bar{q}$ selections of reference [1] are used as the basis of the $W^+W^-\gamma$ selections³. For $W^+W^-(\gamma) \rightarrow \ell^+\nu_\ell\ell^-\bar{\nu}_\ell\gamma$ and $W^+W^-(\gamma) \rightarrow q\bar{q}\ell\bar{\nu}_\ell\gamma$

³Reference [1] refers to the event selection at $\sqrt{s} = 189$ GeV. For data recorded at higher centre-of-mass energies the same likelihood selection is used but with reference distributions obtained from Monte Carlo events

the standard selections are applied. For $W^+W^-(\gamma) \rightarrow q\bar{q}q\bar{q}\gamma$ events, a modified version of the $W^+W^- \rightarrow q\bar{q}q\bar{q}$ selection of reference [1] is used. In the standard selection, events are forced into four jets using the Durham k_T algorithm [21]. In approximately 10 % of Monte Carlo events with high energy photons ($E_\gamma > 10$ GeV), the photon alone forms one of the four jets. This introduces an additional inefficiency, due to the requirement in the preselection that there should be at least one charged particle track associated with each jet. For this reason, events failing the standard $W^+W^- \rightarrow q\bar{q}q\bar{q}$ selection are forced into four jets after excluding the highest energy isolated electromagnetic calorimeter cluster and the selection re-applied. The overall selection efficiency for $W^+W^- \gamma$ events within the signal definition is 88 % and is approximately independent of centre-of-mass energies for $180 \text{ GeV} < \sqrt{s} < 209 \text{ GeV}$.

4.2 Photon Identification

Photon identification is similar to that described in [22], although for this study the minimum photon energy is reduced to 2.5 GeV. Photon candidates are identified as one of three types:

- Unassociated ECAL clusters defined by the requirement that no charged particle track, when extrapolated to the front-face of the ECAL, lies within a distance defined by the typical angular resolution of the ECAL cluster. The lateral spread of the cluster was required to satisfy the criteria described in reference [22].
- Two-track photon conversions which are selected using an artificial neural network as described in [23].
- Conversions where only a single track is reconstructed, identified as an electromagnetic calorimeter cluster associated with a track which is consistent with originating from a photon conversion. The track is required to have no associated hits in either layer of the silicon micro-vertex detector or in the first six layers of the central vertex chamber.

For both types of conversion, the photon energy is defined by the sum of cluster energies pointed to by the track(s).

Photon candidates identified using the above criteria are required to satisfy isolation requirements. The summed energies of any additional tracks and clusters in a 20° half-angle cone defined by the photon direction have to be less than 2 GeV. In addition, the energy deposited in the hadron calorimeter in a 20° half-angle cone around the photon candidate is required to be less than 5 GeV. If the invariant mass formed from the photon candidate and the energy deposit in any ECAL cluster is less than $0.25 \text{ GeV}/c^2$ the candidate is rejected in order to suppress photons from π^0 decay. For photon candidates with $2.5 \text{ GeV} < E_\gamma < 10.0 \text{ GeV}$ a relative likelihood selection is applied to reduce the background from photons from the decays of hadrons (dominated by π^0 and η decays). The likelihood is based on five discriminant variables: E_γ , $|\cos\theta_\gamma|$, the angle between the photon and the nearest jet, the angle between the photon and the nearest track, and the minimum invariant mass formed from the photon candidate and any other ECAL cluster in the event. For photons above 10 GeV the background is low and no photon identification likelihood is needed.

4.3 Photon Acceptance

The identified photon is required to lie within the polar acceptance, generated at higher centre-of-mass energies.

- $|\cos \theta_\gamma| < 0.975$.

The photon is also required to be isolated from the charged fermions in the final state. Cuts are applied on the cosine of the angle between the photon and closest jet, $\cos \theta_{\gamma\text{-JET}}$, and on the cosine of the angle between the photon and a charged lepton from the W-boson decay, $\cos \theta_{\gamma\ell}$:

- $\cos \theta_{\gamma\text{-JET}} < 0.9$ for $W^+W^- \rightarrow q\bar{q}\ell\bar{\nu}_\ell\gamma$ and $W^+W^- \rightarrow q\bar{q}q\bar{q}\gamma$ events,
- $\cos \theta_{\gamma\ell} < 0.9$ for $W^+W^- \rightarrow \ell^+\nu_\ell\ell^-\bar{\nu}_\ell\gamma$ and $W^+W^- \rightarrow q\bar{q}\ell\bar{\nu}_\ell\gamma$ events.

For selected events with photons within the generator level acceptance the photon identification efficiency is 75 % for $E_\gamma \geq 7.5$ GeV, 69 % for $5.0 \text{ GeV} \leq E_\gamma < 7.5$ GeV and 45 % for $2.5 \text{ GeV} \leq E_\gamma < 5.0$ GeV. The photon identification efficiency is almost independent of $\cos \theta_\gamma$ in the region $|\cos \theta_\gamma| < 0.975$. The non-photonic backgrounds are less than 4 % for $|\cos \theta_\gamma| < 0.95$. For $|\cos \theta_\gamma| > 0.95$ the background increases to 8 %. If more than one photon candidate passes the photon acceptance requirements only the highest energy photon is retained for the following analysis.

4.4 Kinematic Requirements

The photon in selected $W^+W^-\gamma$ events is classified as ISR, FSR from the lepton, or as being associated with a jet (either FSR from the parton shower or coming from hadron decay). No special treatment is made for WSR because WSR diagrams are only observable through interference with ISR diagrams and, consequently, the effects of WSR diagrams will be apparent in the event sample classified as ISR. In $\ell^+\nu_\ell\ell^-\bar{\nu}_\ell$ events, photons are classified as ISR if $\cos \theta_{\gamma\ell} < |\cos \theta_\gamma|$, otherwise the photons are classified as FSR from one of the charged leptons. For the $q\bar{q}\ell\bar{\nu}_\ell$ and $q\bar{q}q\bar{q}$ channels the classification is performed using a relative likelihood selection in which kinematic fitting plays a major rôle. Three kinematic fits are employed, corresponding to the following hypotheses:

- a) the photon originates from FSR from the quark; the fit assumes a two-body W^+W^- final state, where the identified photon is included as part of the nearest jet.
- b) the photon originates from FSR from the lepton (only used for $W^+W^-(\gamma) \rightarrow q\bar{q}\ell\bar{\nu}_\ell\gamma$ events); the fit assumes a two-body W^+W^- final state, where the photon is associated with the charged lepton.
- c) the photon originates from ISR; the fit assumes a three body final state consisting of the two W-bosons and the photon.

In each case, the constraints of energy and momentum conservation are imposed and the two reconstructed masses of the W-boson candidates are required to be equal [24]. An event is considered consistent with one of the above hypotheses if the fit converges with a fit probability of greater than 0.1 % and if the reconstructed W-boson mass is greater than 74 GeV. In fully hadronic events there are three possible jet-pairing combinations. Here, for each fit hypothesis, the combination yielding the highest kinematic fit probability is used.

The reconstructed W-boson mass from the three kinematic fit hypotheses along with the cosine of the angle between the photon and the nearest jet are used as the inputs to the relative likelihood. For $q\bar{q}\ell\bar{\nu}_\ell$ events the cosine of the angle between the photon and the charged lepton is also used. The distributions used in the relative likelihood classification are shown in

Figure 1. Good agreement between data and simulation is observed. Three relative likelihoods are constructed and events are classified as being either from ISR, FSR from the charged lepton or radiation associated with the jets. The resulting ISR relative likelihood distribution, \mathcal{L}_{ISR} is shown in Figure 1f. Events are classified as ISR if $\mathcal{L}_{ISR} > \mathcal{L}_{FSR}$ and $\mathcal{L}_{ISR} > \mathcal{L}_{JET}$, where \mathcal{L}_{FSR} and \mathcal{L}_{JET} are the relative likelihoods for the respective hypotheses of FSR and radiation associated with the jets. Only those $W^+W^-\gamma$ candidate events classified as ISR are retained for the analysis. These events are consistent with on-shell W-bosons (fit c), $M_{f_1\bar{f}_2} \sim M_{f_3\bar{f}_4} \sim M_W$ and an isolated photon. This procedure suppresses events with final state radiation and events where the photon is from hadron decay. It also significantly reduces background from $e^+e^- \rightarrow q\bar{q}\gamma$. As a result the systematic uncertainties from photons associated with jets (FSR and π^0/η decays) are greatly reduced.

The application of the above kinematic requirements retains approximately 75 % of selected signal $W^+W^-\gamma$ events with an identified photon (using the definition of Section 3) whilst rejecting 85 % – 98 % (increasing with the photon energy) of events with photons either from FSR or from the decays of mesons.

5 Measurement of the $W^+W^-\gamma$ cross-section

Using the selection criteria defined in the previous section, 187 $W^+W^-\gamma$ events with $E_\gamma > 2.5$ GeV are selected compared to the KandY expectation of 188.4 ± 1.0 events (where the error on the expectation is the quadrature sum of the MC statistical error and luminosity error). Figure 2a shows the photon energy spectrum for the selected $W^+W^-\gamma$ events. Figure 2b shows the distribution of $|\cos \theta_\gamma|$ and Figure 2c shows the distribution of the cosine of the angle between the photon and the nearest charged fermion from the reconstructed W-decay (*i.e.* lepton or jet) in the event. Good agreement between data and Monte Carlo is observed for all distributions. The effect of an anomalous QGC on the photon energy and polar angle distributions is also shown.

The $W^+W^-\gamma$ cross-section is determined within the acceptance defined in Section 3 for the five mean centre-of-mass energies listed in Table 1. The $W^+W^-\gamma$ cross-section is calculated from

$$\hat{\sigma}_{WW\gamma} = \frac{(N_{\text{obs}} - \sigma_{\text{BGD}}\mathcal{L})}{c_{WW\gamma}\varepsilon_{WW\gamma}\mathcal{L}},$$

where N_{obs} is the accepted number of events, σ_{BGD} is the SM background cross-section and \mathcal{L} is the integrated luminosity. The selection efficiency for events generated within the acceptance defined in Section 3, $\varepsilon_{WW\gamma}$, is evaluated using KandY MC $W^+W^-\gamma$ events. Background from migration of $W^+W^-\gamma$ events from just outside the signal region into the selected event sample due to finite detector resolution is accounted for by a factor $c_{WW\gamma}$. This allows the contribution from selected $W^+W^-\gamma$ events outside the signal definition but within the acceptance $E_\gamma > 2.0$ GeV and $|\cos \theta_\gamma| < 0.98$ to scale with the measured cross-section (in contrast to treating this component as background which is fixed by Monte Carlo expectation). The selection efficiency, $\varepsilon_{WW\gamma}$, varies from 41 % – 47 % increasing with centre-of-mass energy. The correction factor, $c_{WW\gamma}$, is 1.14 and is almost independent of centre-of-mass energy. The background cross-section, σ_{BGD} , is estimated using KandY and KK2F. The background from W^+W^- events with photons associated with the jets, including photons from FSR from the parton-shower, is scaled by a factor of 1.30 ± 0.15 , as described in Section 5.1, to account for known discrepancies between data and the JETSET prediction. The Monte Carlo predicts that 24 % of the selected

event sample arises from background processes (including photons associated with jets). The results are listed in Table 2 where they are compared to the predictions from KandY, and are displayed in Figure 3. The systematic uncertainties are described in Section 5.1. For the purpose of combination with the other LEP experiments, the results for a more restrictive signal acceptance are given in the Appendix.

$\langle \sqrt{s} \rangle / \text{GeV}$	$\hat{\sigma}_{\text{WW}\gamma} / \text{fb}$	
	Data	KandY
182.68	$277 \pm 117 \pm 13$	327 ± 3
188.63	$388 \pm 74 \pm 17$	378 ± 4
194.44	$255 \pm 84 \pm 15$	411 ± 4
200.21	$459 \pm 100 \pm 20$	427 ± 4
205.92	$489 \pm 73 \pm 21$	443 ± 4

Table 2: $W^+W^-\gamma$ cross-section measurements for the five centre-of-mass energies listed in Table 1. The errors on the measurements are statistical and systematic respectively. The errors on the KandY expectations are due to limited Monte Carlo statistics.

Table 3 shows the ratio of measured to predicted $W^+W^-\gamma$ cross-sections averaged over the five values of \sqrt{s} for the theoretical predictions from KandY, RacoonWW, EEWWG and KORALW. For RacoonWW, FSR from the parton shower is included as signal since, unlike for KandY and KORALW, there is no way of removing its contribution at the generator level. As a consequence of the uncertainties of the modelling of photons from the parton shower this results in an increased systematic uncertainty as discussed in Section 5.1. For EEWWG, which does not include any FSR, the expectation for the contribution from FSR from leptons (which is considered signal) is taken from PHOTOS. The experimental results correspond to a measurement with 10 % precision of the $W^+W^-\gamma$ cross-section. The best agreement is obtained with KandY and RacoonWW; however, the measurements are of insufficient statistical precision to distinguish between the different calculations. The OPAL result is two standard deviations below the prediction of KORALW. Although the statistical significance is low, the $\mathcal{O}(\alpha)$ NL electroweak corrections of YFSWW implemented in KandY improve the agreement between data and Monte Carlo (the dominant effect is the inclusion of radiation from the W-bosons, specifically its interference with ISR).

	Data/Theory
KandY	$0.99 \pm 0.09 \pm 0.04$
RacoonWW	$0.98 \pm 0.09 \pm 0.06$
EEWWG	$0.91 \pm 0.09 \pm 0.04$
KORALW	$0.84 \pm 0.08 \pm 0.04$

Table 3: The ratios of the experimental to expected SM $W^+W^-\gamma$ cross-sections averaged over \sqrt{s} for four theoretical calculations. The errors are from the statistical and systematic uncertainties on the measurement of the $W^+W^-\gamma$ cross-section.

New physics could appear as resonant structure in the $W\gamma$ invariant mass distribution (for example the decay of an excited W-boson, $W^* \rightarrow W\gamma$). To investigate this possibility, for $q\bar{q}\ell\bar{\nu}_\ell\gamma$ and $q\bar{q}q\bar{q}\gamma$ candidates the invariant masses of the two $W^\pm\gamma$ combinations in selected $W^+W^-\gamma$

events are obtained from an additional kinematic fit. The fit uses the constraints of energy and momentum conservation and the constraint that the invariant masses of the reconstructed $f_1\bar{f}_2$ and $f_3\bar{f}_4$ systems are both equal to the W-mass (previously the requirement was that both masses be equal). Only events for which the kinematic fit converges are retained. For MC events this cut rejects approximately 16 % of selected signal events. The $W\gamma$ invariant mass is calculated from the four-momenta of the four fermions and the photon returned by the fit. Figure 4 shows the reconstructed invariant mass distribution for the two $W^\pm\gamma$ combinations for selected $W^+W^-\gamma$ events with $E_\gamma > 2.5$ GeV. No resonant structure is observed. The data from the region $|\cos\theta_\gamma| < 0.80$, where any contribution from new physics might be expected to be most apparent are also shown.

5.1 Systematic Uncertainties

The contributions to the systematic uncertainties on the $W^+W^-\gamma$ cross-sections for the five values of \sqrt{s} are listed in Table 4 and are described below. The total systematic errors are taken as the sum in quadrature of these components. When determining the average ratio of data to MC the systematic error components for the five energies are taken to be 100 % correlated.

Systematic Uncertainty on $\hat{\sigma}_{WW\gamma}/\text{fb}$						
Error Source	Variation	$\langle\sqrt{s}\rangle/\text{GeV}$				
		183	189	195	201	206
Photons from jets	± 15 %	9	10	12	13	13
Photon energy scale	± 4 %	6	8	5	9	10
Photon angular acceptance	± 5 mrad	4	6	4	7	7
Photon energy resolution	± 10 %	3	4	3	5	5
W^+W^- Selection	± 1.1 %	3	4	3	5	5
Photon Identification	± 1.0 %	3	4	3	5	5
Photon Isolation	± 1.0 %	3	4	3	5	5
$q\bar{q}$ Background	± 6.5 %	2	2	3	3	3
Kinematic Fits	± 0.5 %	1	2	1	2	2
Monte Carlo Statistics	± 0.4 %	1	2	1	2	2
Luminosity	± 0.3 %	1	1	1	1	1
Total Systematic Error		13	17	15	20	21
Statistical Error		117	74	84	100	73

Table 4: The contributions to the experimental error on the $W^+W^-\gamma$ cross-section for the five different values of \sqrt{s} . The systematic variations on the various sources of error are indicated.

Modelling of photons from jets: The modelling of photon candidates associated with the hadronic jets (both from FSR and from π^0 and η decays) is studied by comparing the rate at which photons are identified in $Z^0 \rightarrow q\bar{q}$ events to the PYTHIA prediction (for this comparison data recorded at $\sqrt{s} \sim M_{Z^0}$ during the 1998 – 2000 operation of the LEP accelerator are used). For $2.5 \text{ GeV} < E_\gamma < 20 \text{ GeV}$, there are (38 ± 2) % more photon candidates identified in the data than expected from the Monte Carlo. Above 20 GeV the data are consistent with the Monte Carlo expectation. The ratio of data to Monte Carlo is used to estimate an energy-dependent correction (in photon energy bins of 2.5 GeV) to the Monte Carlo expectation for

the background from W^+W^- events with photons associated with jets. After the $W^+W^- \gamma$ event selection, this corresponds to a (30 ± 2) % correction to the background from photons from jets⁴. Half the size of the correction is propagated as a systematic uncertainty. In the evaluation of the other systematic uncertainties all comparisons between data and MC are performed after making this correction.

ECAL energy scale: A bias in the energy scale for photons (data relative to Monte Carlo) in the region of the energy cut, *i.e.* $E_\gamma \sim 2.5$ GeV, would result in a systematic bias in the $W^+W^- \gamma$ cross-section measurement. The uncertainty on the ECAL energy scale for photons in this region is estimated by examining photons from π^0 decays in $e^+e^- \rightarrow q\bar{q}$ events recorded at $\sqrt{s} \sim M_{Z^0}$ during 1998–2000 and $e^+e^- \rightarrow q\bar{q}(\gamma)$ events recorded at $\sqrt{s} > 180$ GeV. The mean reconstructed π^0 mass for π^0 candidates containing a photon with $2 \text{ GeV} < E_\gamma < 3 \text{ GeV}$ is (142 ± 2) MeV/ c^2 in data compared to 137 MeV/ c^2 in Monte Carlo. As a result a 4 % systematic uncertainty on the ECAL energy scale in the region of $E_\gamma \sim 2.5$ GeV is assigned. The resulting systematic uncertainty on the cross-section is 2 %.

Photon Angular Acceptance: The systematic error associated with the requirement of $|\cos \theta_\gamma| < 0.975$ depends on the accuracy of the Monte Carlo simulation of the angular reconstruction from ECAL clusters at the edge of the acceptance. By comparing the reconstructed polar angle from different detectors (ECAL, tracking, muon chambers) the ECAL acceptance is known to ± 3 mrad out to $|\cos \theta_\gamma| < 0.96$. Beyond the tracking acceptance it is not possible to make this comparison. Therefore a 5 mrad uncertainty on the edge of the acceptance is assigned.

As a cross-check a sample of ISR photons from $e^+e^- \rightarrow q\bar{q}(\gamma)$ events is used. Multi-hadronic events recorded at $180 \text{ GeV} < \sqrt{s} < 209 \text{ GeV}$ are selected [25]. Photons are identified using the same criteria as for the $W^+W^- \gamma$ cross-section analysis. In the data 241 photons are reconstructed in the region $0.950 < |\cos \theta_\gamma| < 0.975$ compared to the Monte Carlo expectation of 237.1. A 5 mrad bias between data and Monte Carlo would result in an expected discrepancy of 28.5 events in this region. The good agreement between data and Monte Carlo provides confirmation that the assigned uncertainty of 5 mrad is reasonable.

ECAL energy resolution: The systematic error from the uncertainty in the ECAL energy resolution is obtained in a similar manner as that used for the ECAL energy scale using the same π^0 sample. There is no evidence for a difference between data and Monte Carlo within the statistical precision of the comparison (± 10 %). The precision of this comparison is used to assign a (10 %) uncertainty the energy resolution, which, when propagated to the uncertainty on the $W^+W^- \gamma$ cross-section yields a systematic error of ± 1 %.

W^+W^- selection efficiency: Systematic uncertainties in the W^+W^- event selection will result in corresponding uncertainties in the $W^+W^- \gamma$ event selection. The estimated systematic uncertainty on the W^+W^- selection efficiency is 1.1 % [1], where the largest uncertainties are

⁴For the comparison with RacoonWW given in Table 3 the systematic errors from photons from jets are calculated differently. In RacoonWW it is impossible to separate photons from FSR from quarks from other diagrams. Consequently the signal definition is modified to include all FSR photons within the theoretical acceptance cuts. In this case the data/MC discrepancy for photons from jets in $Z^0 \rightarrow q\bar{q}$ may either be assigned to a mis-modelling of FSR (signal) or to a mis-modelling of hadron production rate (background). Consequently the systematic uncertainties are larger than for the case when FSR from quarks is also treated as background. The central value for the RacoonWW comparison uses the average of the results obtained and half the difference is assigned as a systematic error.

related to the QCD and fragmentation modelling of jets. For the data sample considered here, the W^+W^- event selection yields 11752 events which is statistically compatible with the Monte Carlo expectation of 11670 ± 58 (where the error is taken to be the theoretical uncertainty on the CC03 cross-section). The difference is consistent with the quoted systematic error of 1.1 %.

Photon Identification: A systematic uncertainty of 1 % is assigned to cover the uncertainties in the simulation of the photon conversion rate and the accuracy of the simulation of the electromagnetic cluster shape [26]. Systematic uncertainties arising from the isolation requirements are discussed below. The efficiency obtained from KandY is consistent with that from KORALW and no additional systematic uncertainty is assigned.

Photon Isolation: The systematic error associated with the isolation requirements depends on the accuracy of the Monte Carlo simulation of the fragmentation process in hadronic jets. This is verified in $Z^0 \rightarrow q\bar{q}$ events recorded at $\sqrt{s} \sim M_{Z^0}$ during 1998 – 2000. For each selected event, the inefficiency of the isolation requirements is determined for random orientations of the isolation cone and parametrised as a function of the angle between the cone and the nearest jet. For all jet-cone angles the inefficiency in the Monte Carlo and data agree to better than 1 %, consequently a 1 % systematic error is assigned. Consistent results, albeit with lower statistical precision, are obtained from $W^+W^- \rightarrow q\bar{q}\ell\bar{\nu}_\ell$ events.

As a cross-check of the photon identification and isolation requirements the sample of reconstructed photons in $e^+e^- \rightarrow q\bar{q}(\gamma)$ events is used. The ratio of the number of reconstructed photons with $2.5 \text{ GeV} < E_\gamma < 50 \text{ GeV}$ in the data to the Monte Carlo expectation is 1.015 ± 0.023 . Good agreement is observed over all $\cos\theta_\gamma$. Due to the limited statistical sensitivity of this test no additional systematic uncertainty is assigned to the photon identification/isolation efficiency.

$q\bar{q}\gamma$ background: The dominant source of non- W^+W^- background is from $e^+e^- \rightarrow Z^0/\gamma \rightarrow q\bar{q}\gamma$ where the identified photon candidate is a genuine photon from ISR. Uncertainties in the modelling of QCD/fragmentation lead to systematic uncertainties in the level of background from $e^+e^- \rightarrow q\bar{q}\gamma$ events in the W^+W^- event selection [1]. As a result the $q\bar{q}\gamma$ background in the $W^+W^- \gamma$ selection is uncertain to 6.0 %. An additional systematic error of 2.5 % arises from the uncertainties in the modelling of ISR in $e^+e^- \rightarrow q\bar{q}\gamma$ events.

Kinematic Fits: The $W^+W^- \gamma$ event selections require that a kinematic fit converges and has a reasonable probability. Possible mis-modelling of the detector response/resolution could result in a difference in the rates at which the fits fail for data and Monte Carlo. This was checked by applying the kinematic fits used in the W mass analysis to all selected W^+W^- events and comparing the failure rates for data and Monte Carlo. The efficiency ($q\bar{q}\ell\bar{\nu}_\ell$ and $q\bar{q}q\bar{q}$ combined) in data is $(83.9 \pm 0.4) \%$ compared with the Monte Carlo expectation of 84.1 %. The ratio of these efficiencies is 0.997 ± 0.005 and, consequently, a systematic uncertainty of 0.5 % is assigned.

Monte Carlo Statistics: The effect of finite Monte Carlo statistics is taken into account and leads to 0.3 % systematic uncertainties on the measured cross-sections.

Luminosity: The total uncertainty on the integrated luminosity of the data samples is 0.3 %, dominated by systematics.

6 Limits on M_W $\mathcal{O}(\alpha)$ Systematic Uncertainties

The anticipated experimental error on M_W from LEP2 is approximately 35 MeV. A potential source of theoretical uncertainty is the treatment of higher order QED corrections in the Monte Carlo programs used to simulate the process $e^+e^- \rightarrow 4f(\gamma)$. A recent estimate suggests a total theoretical systematic uncertainty due to $\mathcal{O}(\alpha)$ effects of 5 MeV [7]. However, as pointed out by the authors [7], this estimate is based upon the invariant mass of the $\mu^-\bar{\nu}_\mu$ system in $e^+e^- \rightarrow \mu^-\bar{\nu}_\mu u\bar{d}(\gamma)$ events, whereas the experimental procedure used to extract M_W is complicated by the fact that the four LEP collaborations use kinematic fits to improve significantly the event-by-event W-mass resolution [27–30]. One effect of the kinematic fit is to constrain the total energy of the reconstructed fermions to \sqrt{s} . For events with photons from ISR this procedure introduces a bias in the reconstructed W-mass as the energies of four fermions should be constrained to $\sqrt{s'}$, the centre-of-mass energy after photon radiation, rather than to \sqrt{s} . Consequently, as a result of the experimental procedure used to extract M_W , the $\mathcal{O}(\alpha)$ theoretical systematic uncertainties may be significantly greater than those obtained by considering the invariant mass distribution of the final state fermions [31].

6.1 QED and Electroweak Corrections in Kandy

In the Kandy generator it is possible to study the effects of different theoretical corrections using event correction weights [9] which, when used to weight generated events, allow different theoretical predictions to be tested. By processing generated fully-simulated events through the full OPAL W-mass analysis it is possible to determine the W-mass biases associated with these corrections. For example, degrading the $\mathcal{O}(\alpha^3)$ exponentiated LL treatment of collinear ISR to $\mathcal{O}(\alpha^2)$ results in a systematic bias of less than 1 MeV [7, 30]. In a similar manner the non-leading (NL) $\mathcal{O}(\alpha)$ electroweak corrections, including radiation from the W-bosons, may be switched off using the appropriate event correction weights, w_{NL}^i . When applied to the full OPAL W-mass analysis it is found that dropping the $\mathcal{O}(\alpha)$ NL electroweak corrections results in a shift in the reconstructed W-mass of 15 MeV. This relatively large bias is due to the modification of the $\sqrt{s'}$ distribution rather than a distortion in the invariant mass distribution of the fermion pairs [31]. The change in the $\sqrt{s'}$ distribution is due to the inclusion in Kandy of the diagrams for radiation from the W-bosons which, through interference with the ISR diagrams, reduces the cross-section for the production of real photons [32]⁵. Although the fractional change in $W^+W^-\gamma$ cross-section is largest at $\cos\theta_\gamma = 0$ where the photon production rate is reduced by 30 % [9], in absolute terms the reduction in the cross-section shows no strong $\cos\theta_\gamma$ dependence. Consequently the $W^+W^-\gamma$ cross-section measurement provides a test of the modelling of radiation from the W-bosons (and the interference with ISR) in the Kandy Monte Carlo. Since the largest source of systematic bias from the so-called $\mathcal{O}(\alpha)$ NL corrections is a direct result of the modification of the spectrum of real photons, the associated systematic uncertainties on M_W may be constrained by the measurement of the $W^+W^-\gamma$ cross-section.

6.2 Constraints from the $W^+W^-\gamma$ Measurements

To investigate the experimental limits on possible biases on the measurement of M_W due to photon production away from the collinear region the correction weights from Kandy are first

⁵This effect was investigated by running YFSWW with KEYCOR=2 and KEYCOR=3 switching between the YFS form factor solely for ISR and the full form factor including WSR and interference between WSR and ISR.

expressed in the form

$$w_{NL}^i = 1.0 + \delta_{NL}^i.$$

By modifying the weights to

$$w_{NL}^i = 1.0 + \kappa \delta_{NL}^i$$

it is possible to investigate a continuous range of scenarios. A value of $\kappa = 0$ corresponds to the treatment of $\mathcal{O}(\alpha)$ NL electroweak corrections of YFSWW (*i.e.* the default in KandY) and $\kappa = 1.0$ corresponds to dropping the NL $\mathcal{O}(\alpha)$ corrections. The parameter κ and its errors are obtained from a binned extended maximum likelihood fit to the $|\cos\theta_\gamma|$ distribution of Figure 2, taking into account both the overall normalisation and shape, giving

$$\kappa = 0.38 \pm 0.45 \pm 0.15,$$

where the first error is statistical and the second due to systematic uncertainties in the event selection efficiency. The data favour the KandY prediction including the NL corrections. Most of the sensitivity comes from the photon rate rather than the angular distribution. The measured value of κ suggests that the measured value of M_W from the OPAL W-mass analysis, obtained using KandY as a reference, should be corrected by (-5 ± 6) MeV. Using the measured cross-section alone gives a similar result of (-1 ± 7) MeV. From these studies it is concluded that the systematic error on M_W due to the Monte Carlo implementation of QED diagrams resulting in real photon production away from the collinear region should be not more than 6 MeV.

7 Anomalous Quartic Gauge Boson Couplings

The non-Abelian nature of the electroweak sector of the Standard Model results in vector boson self-interactions. In addition to the triple gauge boson couplings (TGCs), $W^+W^-\gamma$ and $W^+W^-Z^0$, the Standard Model predicts the existence of four quartic gauge couplings, $W^+W^-W^+W^-$, $W^+W^-Z^0Z^0$, $W^+W^-Z^0\gamma$ and $W^+W^-\gamma\gamma$. These couplings are not expected to play a significant role at LEP energies, but will be important at the LHC [33] and at a future TeV linear collider [34].

Quartic gauge boson couplings can be probed in final states with three vector bosons. At LEP centre-of-mass energies, final states involving three massive gauge bosons are kinematically out of reach. However, it is possible to study the processes $e^+e^- \rightarrow W^+W^-\gamma$ [10, 11] and $e^+e^- \rightarrow Z^0\gamma\gamma$ [35]. In the Standard Model, the contribution of the quartic couplings to $e^+e^- \rightarrow W^+W^-\gamma$, shown in Figure 5, is expected to be too small to measure and that to $e^+e^- \rightarrow Z^0\gamma\gamma$ is zero. Nevertheless, it is possible to set direct limits on possible anomalous contributions to the quartic gauge boson couplings.

7.1 Theoretical Framework

In the SM the form and strength of the vector boson self-interactions are fixed by $SU(2) \times U(1)$ gauge invariance. As is the case for triple gauge boson couplings [36], in extensions to the SM, anomalous quartic couplings can be parametrised by additional terms in the Lagrangian [20, 37, 38]. These are required to conserve custodial $SU(2)_c$ symmetry in order to avoid deviations

of the ρ parameter⁶ from the experimentally well established value close to 1. Only operators which do not introduce anomalous triple gauge couplings are considered. For example, the anomalous quadrupole moment operator generates both $W^+W^-\gamma$ and $W^+W^-\gamma\gamma$ couplings. Therefore, it is not considered as a source of genuine anomalous quartic couplings since its strength, λ_γ , is already tightly constrained from the study of TGCs at LEP [39, 40] and at the Tevatron [41]. The lowest dimension operators which generate genuine anomalous quartic couplings involving photons are of dimension six. Three such possibilities are considered here, \mathcal{L}_6^0 , \mathcal{L}_6^c [37] and \mathcal{L}_6^n [20, 42]:

$$\begin{aligned}\mathcal{L}_6^0 &= -\frac{e^2}{16\Lambda^2}a_0F^{\mu\nu}F_{\mu\nu}\vec{W}^\alpha\cdot\vec{W}_\alpha, \\ \mathcal{L}_6^c &= -\frac{e^2}{16\Lambda^2}a_cF^{\mu\alpha}F_{\mu\beta}\vec{W}^\beta\cdot\vec{W}_\alpha, \\ \mathcal{L}_6^n &= i\frac{e^2}{16\Lambda^2}a_n\epsilon_{ijk}W_{\mu\alpha}^{(i)}W_\nu^{(j)}W^{(k)\alpha}F^{\mu\nu},\end{aligned}$$

with

$$\vec{W}_\mu = \begin{pmatrix} \frac{1}{\sqrt{2}}(W_\mu^+ + W_\mu^-) \\ \frac{i}{\sqrt{2}}(W_\mu^+ - W_\mu^-) \\ Z_\mu/\cos\theta_W \end{pmatrix},$$

where $F^{\mu\nu}$ and $W^{\mu\nu}$ are the field strength tensors of the photon and W fields respectively. Both \mathcal{L}_6^0 and \mathcal{L}_6^c , which conserve C and P (separately), generate anomalous $W^+W^-\gamma\gamma$ and $Z^0Z^0\gamma\gamma$ couplings. The CP violating term \mathcal{L}_6^n results in an anomalous $W^+W^-\gamma Z^0$ coupling. In each case, the strength of the coupling is proportional to a_i/Λ^2 , where Λ represents a scale for new physics. A more general description of the operators leading to anomalous quartic couplings accessible at LEP can be found in the paper of Bélanger *et al.* [43]. The two additional dimension 6 operators, parametrised by \hat{a}_0 and \hat{a}_c , identified by Denner *et al.* [44] are not considered here as the effects of \hat{a}_0 and \hat{a}_c are almost identical to those of a_0 and a_c , respectively.

7.2 Experimental Limits

The selected $W^+W^-\gamma$ events are used to set limits on possible anomalous contributions to the $W^+W^-\gamma\gamma$ and $W^+W^-\gamma Z^0$ quartic gauge couplings. The limits are extracted from the measured differential cross-section as a function of the photon energy and photon polar angle. The signal of anomalous quartic gauge boson couplings at LEP would be an excess of $W^+W^-\gamma$ events. The effect of anomalous QGCs increases with photon energy. Furthermore, the sensitivity to anomalous QGCs increases with increasing \sqrt{s} .

The calculation of Stirling and Werthenbach [20] allows for the assessment of the impact of anomalous quartic couplings and is implemented in the EEWWG program. This calculation includes the ISR diagrams, the WSR diagrams, the SM QGC diagram and can accommodate anomalous quartic couplings. However, the recent implementation of anomalous QGCs in the RacoonWW [44] and WRAP [45] programs identified a problem with the EEWWG program, indicating that $a_0 \rightarrow -a_0$ and $a_c \rightarrow -a_c$ in EEWWG. In this study the EEWWG program is used with the signs of a_0 and a_c inverted. To set limits on possible anomalous couplings a binned

⁶ $\rho = M_W^2/(M_{Z^0}^2 \cos^2 \theta_W)$, where M_W and M_{Z^0} are the masses of the W^\pm and Z^0 bosons and θ_W is the weak mixing angle.

maximum likelihood fit to the observed distribution of $[E_\gamma, |\cos\theta_\gamma|]$ is performed using bins of $[5 \text{ GeV}, 0.1]$. Fits are performed to the data for the five separate energy ranges of Table 1 and the resulting likelihood curves are summed. The effects of anomalous couplings are introduced by reweighting events generated with KandY using the average ratio of anomalous QGC to SM matrix elements from EEWWG in the relevant bin of $[E_\gamma, |\cos\theta_\gamma|]$. The resulting summed likelihood curves are shown in Figure 6. Results are obtained for three single parameter fits, where one of a_0 , a_c or a_n is varied whilst the other two parameters are set to zero, and a two parameter fit to $\{a_0, a_c\}$. The results include the effect of the experimental systematic errors and assume a 10 % theoretical uncertainty⁷ on the cross-section for $e^+e^- \rightarrow W^+W^-\gamma$. These uncertainties are taken to be 100 % correlated between the five energy ranges. The best fit does not occur at the SM value of zero. However this does not imply the data are inconsistent with the SM. The consistency with the SM prediction, given by the probability of obtaining a value of $-\ln\mathcal{L}$ greater than that observed for $\{a_0 = 0, a_c = 0, a_n = 0\}$, is 19 %. The 95 % confidence level upper limits on the anomalous couplings, obtained from the likelihood curves, $\Delta(\ln\mathcal{L}) = 1.92$, are:

$$\begin{aligned} -0.020 \text{ GeV}^{-2} &< a_0/\Lambda^2 < 0.020 \text{ GeV}^{-2}, \\ -0.053 \text{ GeV}^{-2} &< a_c/\Lambda^2 < 0.037 \text{ GeV}^{-2}, \\ -0.16 \text{ GeV}^{-2} &< a_n/\Lambda^2 < 0.15 \text{ GeV}^{-2}, \end{aligned}$$

For a_c the region $-0.020 \text{ GeV}^{-2} < a_c/\Lambda^2 < -0.002 \text{ GeV}^{-2}$ is also excluded at the 95 % C.L. The derived upper limits are less restrictive than the expected limits. For example, the expected limit on a_0 is $|a_0/\Lambda^2| < 0.014 \text{ GeV}^{-2}$. The limits are worse than expected due to a slight excess of high energy photons in the $\sqrt{s} > 205 \text{ GeV}$ data sample.

8 Conclusions

Using 187 $W^+W^-\gamma$ candidates with photon energies greater than 2.5 GeV the $W^+W^-\gamma$ cross-section is measured at five values of \sqrt{s} . The results are consistent with the Standard Model expectation. Averaging over the five energies, the ratio of the observed cross-section to the prediction of the concurrent Monte Carlo KoralW and YFSWW (KandY) is

$$R(\text{data/MC}) = 0.99 \pm 0.09 \pm 0.04,$$

where the errors represent the statistical and systematic uncertainties respectively. This provides a 10 % test of the KandY implementation of $\mathcal{O}(\alpha)$ effects producing a real photon away from the collinear region. From these studies it is concluded that the systematic error on M_W due to the Monte Carlo implementation of QED diagrams resulting in real photon production away from the collinear region should be not more than 6 MeV.

The data are used to derive 95 % confidence level upper limits on possible anomalous contributions to the $W^+W^-\gamma\gamma$ and $W^+W^-Z^0\gamma$ vertices:

$$\begin{aligned} -0.020 \text{ GeV}^{-2} &< a_0/\Lambda^2 < 0.020 \text{ GeV}^{-2}, \\ -0.053 \text{ GeV}^{-2} &< a_c/\Lambda^2 < 0.037 \text{ GeV}^{-2}, \\ -0.16 \text{ GeV}^{-2} &< a_n/\Lambda^2 < 0.15 \text{ GeV}^{-2}, \end{aligned}$$

where Λ represents the energy scale for new physics.

⁷This represents a conservative estimate of the theoretical uncertainty, comparisons of YFSWW and RacoonWW suggest 5 %.

9 Acknowledgments

We would like to thank James Stirling and Anja Werthenbach for providing the program EEWWG which is used to determine the effects of anomalous couplings in $W^+W^-\gamma$ events. We also greatly appreciate their many useful suggestions and comments. We would also like to thank Markus Roth and the RacoonWW group for providing cross-section calculations using the RacoonWW program. We thank Marius Skrzypek and Wieslaw Płaczek for many useful discussions.

We particularly wish to thank the SL Division for the efficient operation of the LEP accelerator at all energies and for their close cooperation with our experimental group. In addition to the support staff at our own institutions we are pleased to acknowledge the

Department of Energy, USA,

National Science Foundation, USA,

Particle Physics and Astronomy Research Council, UK,

Natural Sciences and Engineering Research Council, Canada,

Israel Science Foundation, administered by the Israel Academy of Science and Humanities,

Benozio Center for High Energy Physics,

Japanese Ministry of Education, Culture, Sports, Science and Technology (MEXT) and a grant under the MEXT International Science Research Program,

Japanese Society for the Promotion of Science (JSPS),

German Israeli Bi-national Science Foundation (GIF),

Bundesministerium für Bildung und Forschung, Germany,

National Research Council of Canada,

Hungarian Foundation for Scientific Research, OTKA T-038240, and T-042864,

The NWO/NATO Fund for Scientific Research, the Netherlands.

10 Appendix

For the purpose of the combination of results from the four LEP experiments cross-section results are obtained for the signal definition:

- $E_\gamma > 5 \text{ GeV}$,
- $|\cos \theta_\gamma| < 0.95$,
- $\cos \theta_{\gamma f} < 0.90$,
- $|M_{f_1\bar{f}_2} - M_W|$ and $|M_{f_3\bar{f}_4} - M_W| < 2 \Gamma_W$.

The experimental cuts on the photon acceptance are modified to match the signal definition. For the modified selection, 124 events are selected, compared to the SM expectation (KandY) of 118.7 ± 0.6 . The results are summarised in Table 5.

$\langle \sqrt{s} \rangle / \text{GeV}$	$\hat{\sigma}_{\text{WW}\gamma} / \text{fb}$	
	Data	KandY
182.68	$102 \pm 60 \pm 5$	141 ± 2
188.63	$163 \pm 41 \pm 6$	175 ± 3
194.44	$166 \pm 57 \pm 7$	201 ± 2
200.21	$214 \pm 60 \pm 7$	216 ± 3
205.92	$298 \pm 50 \pm 8$	226 ± 3

Table 5: $W^+W^-\gamma$ cross-section measurements for the signal definition to be used for a LEP combination of results. The errors are statistical and systematic respectively. The systematic uncertainties are calculated as described in Section 5.1.

References

- [1] OPAL Collaboration, G. Abbiendi *et al.*, Phys. Lett. **B493** (2000) 249.
- [2] ALEPH Collaboration, R. Barate *et al.*, Phys. Lett. **B484** (2000) 205;
DELPHI Collaboration, P. Abreu *et al.*, Phys. Lett. **B479** (2000) 89;
L3 Collaboration, M. Acciarri *et al.*, Phys. Lett. **B496** (2000) 19.
- [3] The LEP Collaborations ALEPH, DELPHI, L3 and OPAL, the LEP Electroweak Working Group and the SLD Heavy Flavour Group, “A Combination of Preliminary Electroweak Measurements and Constraints on the Standard Model”, CERN-EP-2002-091.
- [4] Program YFSWW3, S. Jadach *et al.*, Phys. Lett. **B417** (1998) 326.
- [5] Program RacoonWW, A. Denner, S. Dittmaier, M. Roth and D. Wackeroth, Nucl. Phys. **B560** (1999) 33;
A. Denner, S. Dittmaier, M. Roth and D. Wackeroth, Nucl. Phys. **B587** (2000) 67.
- [6] M. W. Grunewald and G. Passarino *et al.*, “Four-Fermion Production in Electron-Positron Colliders”, CERN-2000-09-A (hep-ph/0005309).
- [7] S. Jadach *et al.*, Phys. Lett. **B523** (2001) 117.
- [8] Program KORALW V1.42, M. Skrzypek *et al.*, Comp. Phys. Comm. **94** (1996) 216;
M. Skrzypek *et al.*, Phys. Lett. **B372** (1996) 289;
M. Skrzypek *et al.*, Comp. Phys. Comm. **119** (1999) 1.
- [9] Program KORALW V1.53 and YFSWW3, S. Jadach *et al.*, Comp. Phys. Comm. **140** (2001) 475.
- [10] OPAL Collaboration, G. Abbiendi *et al.*, Phys. Lett. **B471** (1999) 293.
- [11] L3 Collaboration, P. Achard *et al.*, Phys. Lett. **B527** (2002) 29.
- [12] OPAL Collaboration, K. Ahmet *et al.*, Nucl. Instr. and Meth. **A305** (1991) 275;
OPAL Collaboration, G. Abbiendi *et al.*, Eur. Phys. J. **C14** (2000) 373;
S. Anderson *et al.*, Nucl. Instr. and Meth. **A403** (1998) 326.
- [13] OPAL Collaboration, G. Abbiendi *et al.*, Eur. Phys. J. **C13** (2000) 553.

- [14] J. Allison et al., Nucl. Instr. and Meth. **A317** (1992) 47.
- [15] D. R. Yennie, S. C. Frautschi and H. Suura, Ann. Phys. **13** (1961) 379.
- [16] E. Barberio and Z. Wąs, Comp. Phys. Comm. **79** (1994) 291.
- [17] T. Sjöstrand, Comp. Phys. Comm. **39** (1986) 374;
T. Sjöstrand and M. Bengtsson, Comp. Phys. Comm. **43** (1987) 367.
- [18] A.P. Chapovsky and V.A. Khoze, Eur. Phys. J. **C9** (1999) 449.
- [19] S. Jadach, B.F. Ward and Z. Wąs, Phys. Lett. **B449** (1999) 97.
- [20] W.J. Stirling and A. Werthenbach, Eur. Phys. J. **C14** (2000) 103.
- [21] N. Brown and W.J. Stirling, Phys. Lett. **B252** (1990) 657;
S. Bethke, Z. Kunszt, D. Soper and W.J. Stirling, Nucl. Phys. **B370** (1992) 310;
S. Catani *et al.*, Phys. Lett. **B269** (1991) 432;
N. Brown and W.J. Stirling, Z. Phys. **C53** (1992) 629.
- [22] OPAL Collaboration, K. Ackerstaff *et al.*, Phys. Lett. **B437** (1998) 218.
- [23] OPAL Collaboration, P.D. Acton *et al.*, Z. Phys. **C55** (1992) 191.
- [24] OPAL Collaboration, K. Ackerstaff *et al.*, Eur. Phys. J. **C1** (1998) 395.
- [25] OPAL Collaboration, K. Ackerstaff *et al.*, Eur. Phys. J. **C6** (1999) 1.
- [26] OPAL Collaboration, G. Abbiendi *et al.*, Phys. Lett. **B544** (2001) 29.
- [27] ALEPH Collaboration, R. Barate *et al.*, Eur. Phys. J. **C17** (2000) 241.
- [28] DELPHI Collaboration, P. Abreu *et al.*, Phys. Lett. **B515** (2001) 238.
- [29] L3 Collaboration M. Acciarri *et al.*, Phys. Lett. **B454** (1999) 386.
- [30] OPAL Collaboration, G. Abbiendi *et al.*, Phys. Lett. **B507** (2001) 29.
- [31] M.A. Thomson, “The Influence of the Experimental Methodology on the QED Theoretical Uncertainties on the Measurement of M_W at LEP”, Cavendish-HEP-2003/08, hep-ph/0307043, *submitted to JHEP*.
- [32] W. Płaczek, private communication.
- [33] A.S. Belyaev *et al.*, Phys. Rev. **D59** (1999) 015022.
- [34] E. Boos *et al.*, Phys. Rev. **D57** (1998) 1553.
- [35] L3 Collaboration, P. Achard *et al.*, Phys. Lett. **B540** (2001) 43.
- [36] K. Hagiwara, R.D. Peccei, D. Zeppenfeld and K. Hikasa, Nucl. Phys. **B282** (1987) 253.
- [37] G. Bélanger and F. Boudjema, Phys. Lett. **B288** (1992) 201.
- [38] G. Abu Leil and W.J. Stirling, J. Phys. **G21** (1995) 517.

- [39] OPAL Collaboration, G. Abbiendi *et al.*, Eur. Phys. J. **C19** (2001) 1.
- [40] ALEPH Collaboration, A. Heister *et al.*, Eur. Phys. J. **C21** (2001) 423;
DELPHI Collaboration, P. Abreu *et al.*, Phys. Lett. **B502** (2001) 9;
L3 Collaboration, M. Acciarri *et al.*, Phys. Lett. **B467** (1999) 171.
- [41] CDF Collaboration, F. Abe *et al.*, Phys. Rev. Lett. **78** (1997) 4536;
D0 Collaboration, B. Abbott *et al.*, Phys. Rev. **D58** (1998) 051101.
- [42] O.J.P. Eboli, M.C. González-García and S.F. Novaes, Nucl. Phys. **B411** (1994) 381.
- [43] G. Bélanger *et al.*, Eur. Phys. J. **C13** (2000) 283.
- [44] A. Denner, S. Dittmaier, M. Roth and D. Wackerath, Eur. Phys. J. **C20** (2001) 201.
- [45] G. Montagna *et al.*, Phys. Lett. **B515** (2001) 197.

OPAL

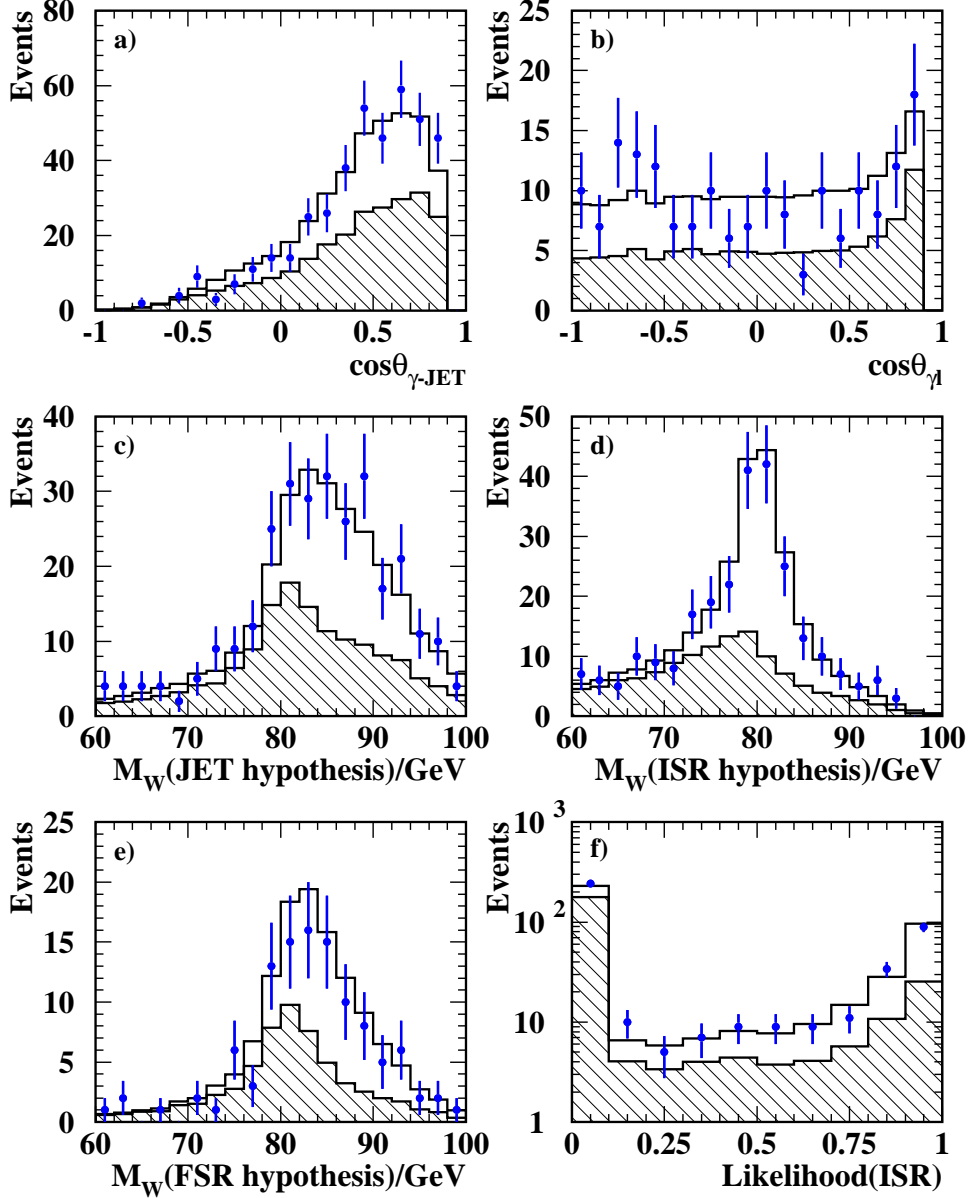


Figure 1: The five kinematic variables used to classify the photon in $W^+W^- \gamma$ events as being from ISR, FSR or associated with the jet. Unless otherwise specified the distributions are shown for $q\bar{q}\ell\bar{\nu}_\ell$ and $q\bar{q}q\bar{q}$ events combined. The variables are: a) the angle between the photon and the nearest jet, $\cos\theta_{\gamma\text{-JET}}$; b) the angle between the photon and the charged lepton, $\cos\theta_{\gamma\ell}$ ($q\bar{q}\ell\bar{\nu}_\ell$ events only); c) the reconstructed W-boson mass under the hypothesis that the photon is associated with jet; d) the reconstructed W-boson mass under the hypothesis that the photon is from ISR; e) the reconstructed W-boson mass under the hypothesis that the photon is from FSR ($q\bar{q}\ell\bar{\nu}_\ell$ only). Plot f) shows the resulting relative likelihood distribution for the ISR hypothesis. In all cases the data are shown by points with error bars, the total SM expectation is shown by the histogram and the contributions from processes other than ISR are shown by the hatched histograms.

OPAL

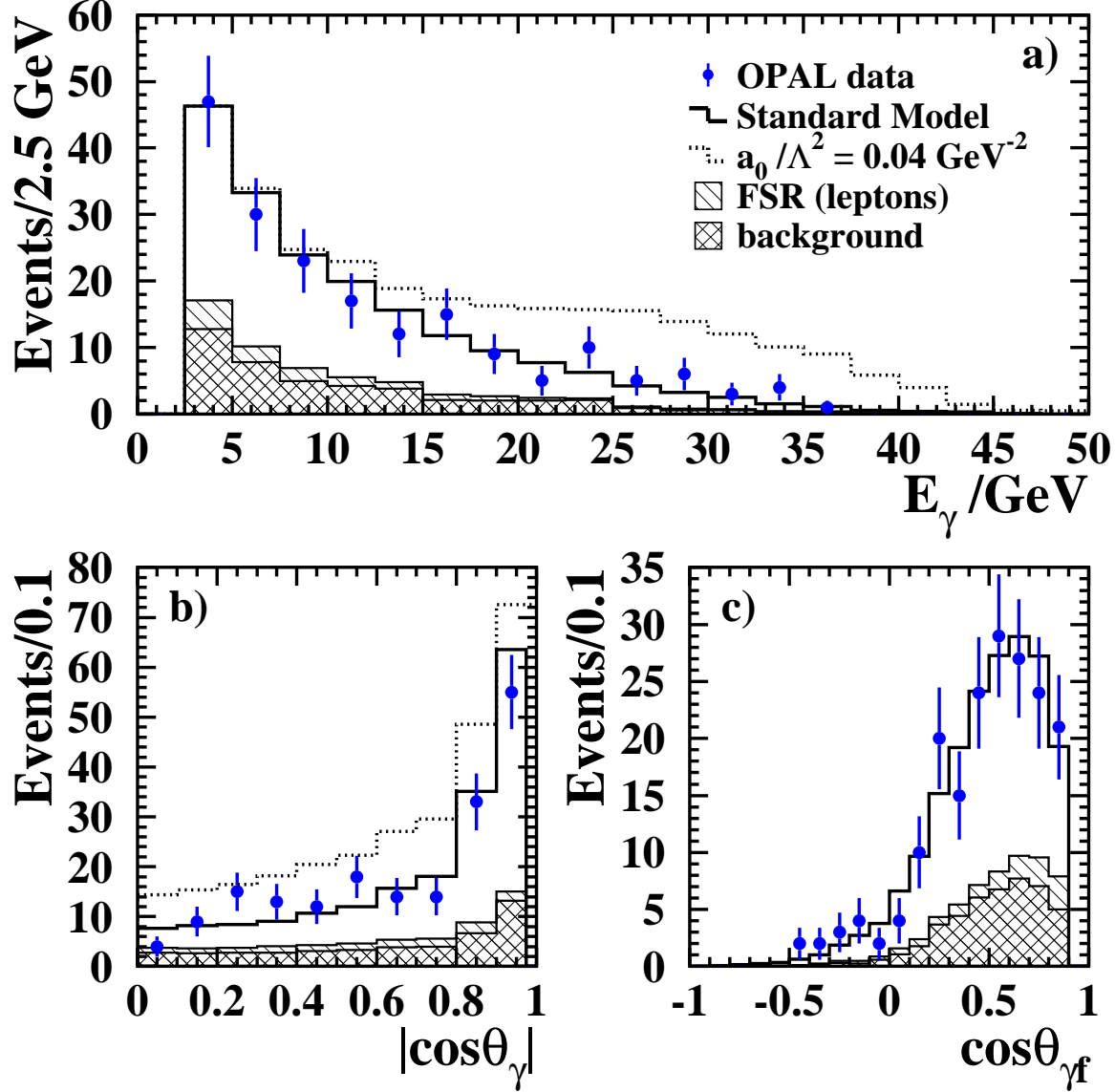


Figure 2: For selected $W^+W^- \gamma$ events ($180 \text{ GeV} < \sqrt{s} < 209 \text{ GeV}$), a) shows the photon energy spectrum, b) the modulus of the cosine of the polar angle of the photon, and c) the cosine of the angle between the photon and the nearest charged fermion. The data are shown by the points with error bars and the SM expectations (Kandy) are shown by the histograms. The doubly-hatched histograms indicate the contributions from non- W^+W^- background and background from photons associated with the parton-shower (either FSR or from hadron decay). The singly-hatched histograms show the contributions from FSR from leptons. The expected E_γ and $|\cos\theta_\gamma|$ distributions for an anomalous QGC of $a_0/\Lambda^2 = 0.040 \text{ GeV}^{-2}$ are also shown.

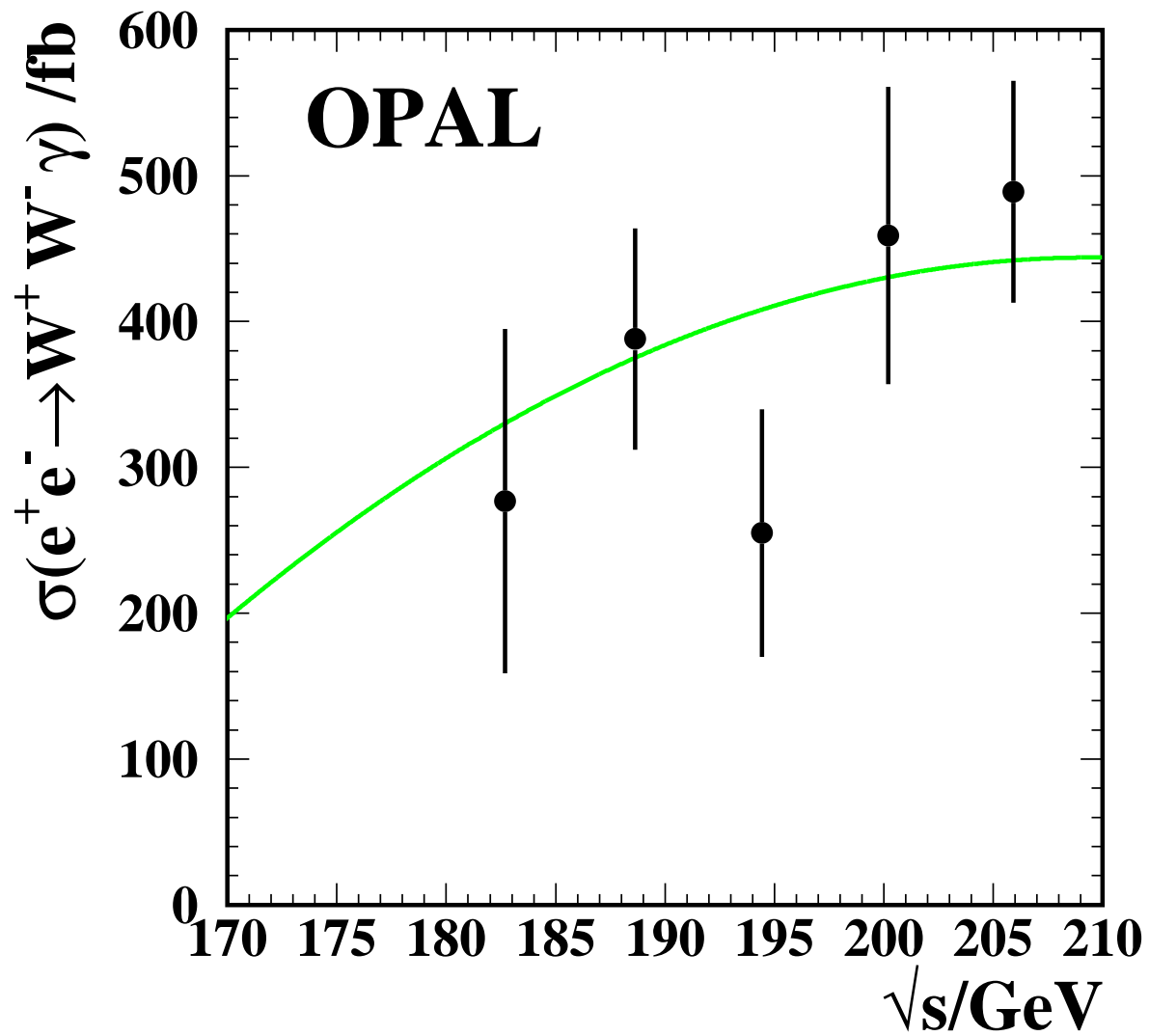


Figure 3: Measured $W^+W^-\gamma$ cross-section for the signal definition of Section 3. The points with error bars show the OPAL measurements. The curve shows the SM expectation obtained from the Kandy program.

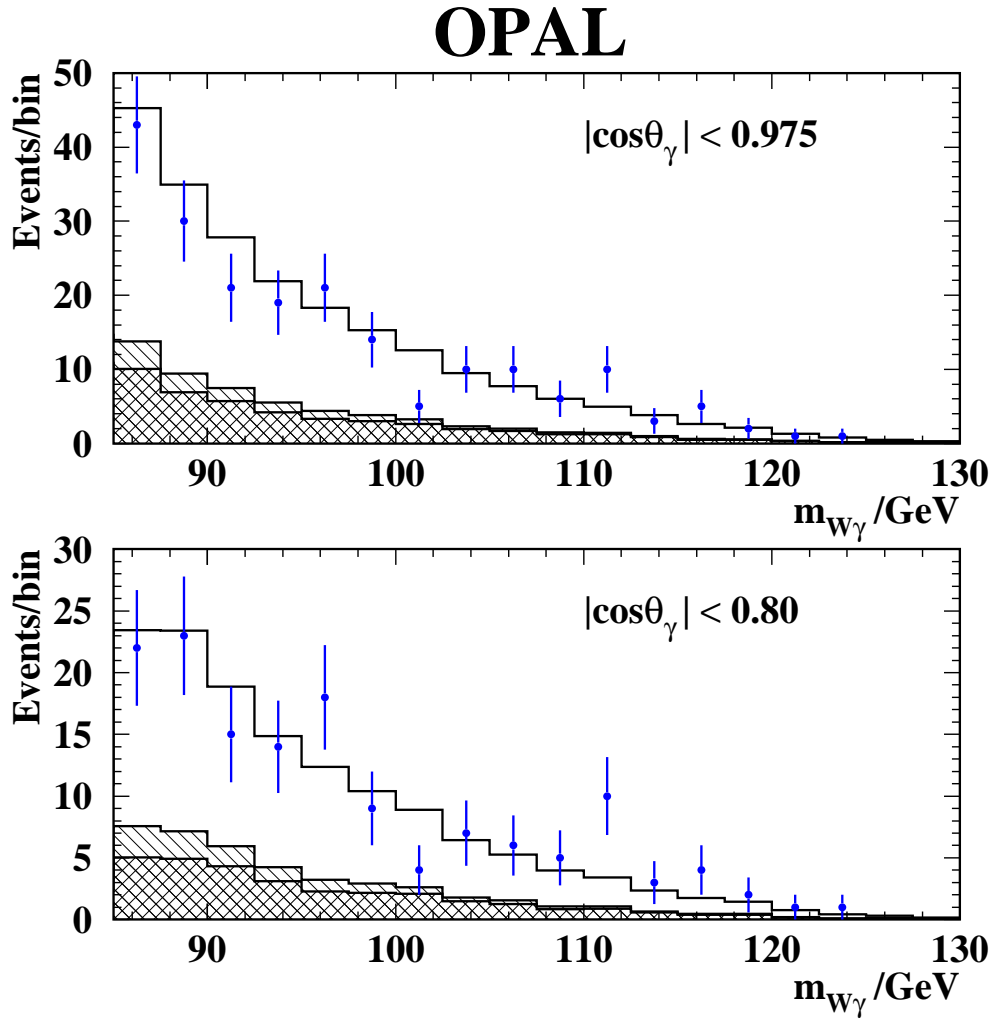


Figure 4: Reconstructed invariant mass of $W^\pm\gamma$ in selected $W^+W^-\gamma$ events with $E_\gamma > 2.5$ GeV (two entries per event). The data are shown by the points, the Standard Model expectation, determined from KandY, is shown by the histogram. The singly hatched histograms show the contribution from FSR from leptons and the doubly hatched histograms show the background.

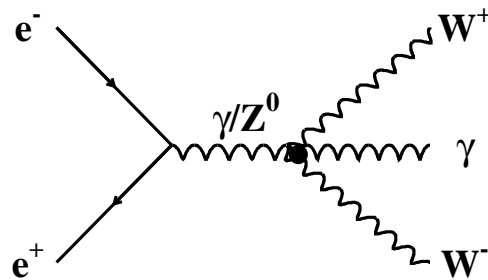


Figure 5: Standard Model production diagram for the $W^+W^-\gamma$ final states involving the $W^+W^-\gamma\gamma$ and $W^+W^-Z^0\gamma$ quartic gauge couplings.

OPAL

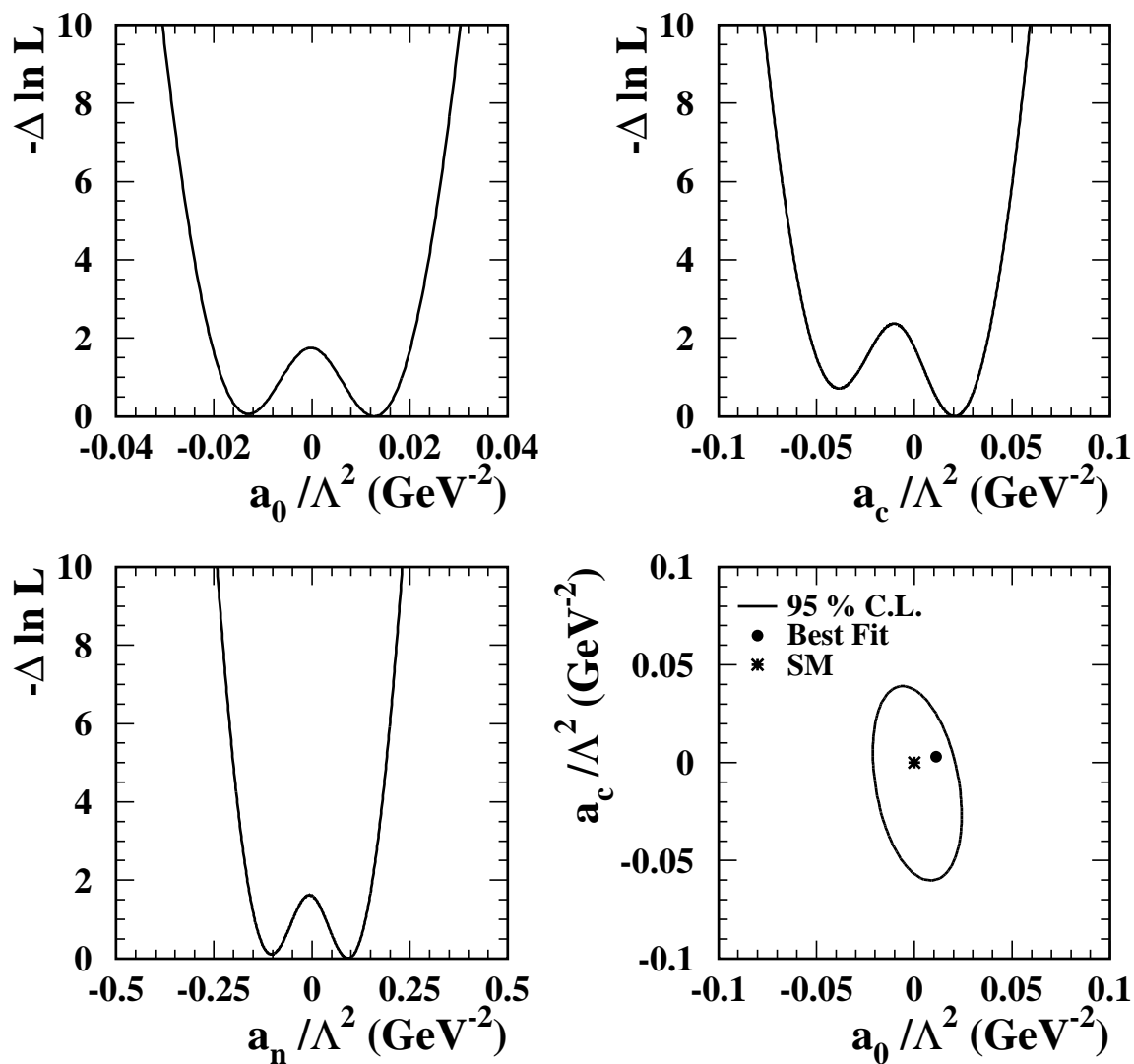


Figure 6: Likelihood curves for the anomalous QGC parameters a_0 , a_c and a_n . Also shown is the 95 % C.L. region for (a_0, a_c) . The curves include the experimental systematic uncertainties and a 10 % theoretical uncertainty for the $e^+e^- \rightarrow W^+W^-\gamma$ cross-section.